Super twisting control for tensegrity systems

José Angel Alvarez Duarte, Juan Manuel Jacinto-Villegas, Adriana Herlinda Vilchis-Gonzalez, Salih Abdelaziz, Juan Carlos Avila Vilchis, Philippe Poignet

Super twisting control for tensegrity systems

José Angel Alvarez Duarte[1,2] Juan Manuel Jacinto Villegas[1,3] Adriana H. Vilchis González[1] Salih Abdelaziz[2] Juan Carlos Avila Vilchis[1]

Philippe Poignet[2]

[1]Facultad de Ingeniería, Universidad Autónoma del Estado de México, Mexico
[2]Laboratoire d'Informatique, de Robotique et de Microéléctronique de Montpellier, Université de Montpellier, France
[3]Cátedras CONACYT, Ciudad de México, Mexico

***Abstract*— This paper reports a super twisting sliding mode control strategy applied to a planar tensegrity system. The main objective is to drive the system to a desired angular position while the tensions in the cables are kept within a predetermined range to preserve the prestressed condition characterizing tensegrity systems. Stability conditions for the proposed control strategy are established and closed-loop stability is demonstrated through numerical simulations and experimental validations. In addition, the stiffness variation of the system has been experimentally performed using the same control strategy. Moreover, robustness to external perturbations using the proposed control strategy has been evaluated.**

Keywords*— *Tensegrity mechanism, Sliding mode control, Nonlinear systems.

I. INTRODUCTION

Tensegrity systems, as prestressed mechanical structures, have dedicated elements working under compression (e.g., rods) and other elements working under tension (e.g., cables). These compliant structures are lightweight systems with inherent stability [1]. As reported in [2] "A tensegrity system is a system in a stable self-equilibrated state comprising a discontinuous set of compressed components inside a continuum of tensioned components." A tensegrity mechanism is an actuated tensegrity structure, performed by either actuating the compressive elements or the tensile elements.

Some open-loop control strategies for tensegrity mechanisms have been introduced in [3] and [4] obtaining a stable equilibrium position using a kinematic approach. These strategies cannot deal with friction effects, nonlinearities, or unmodeled dynamics. Closed-loop control strategies for tensegrity systems have also been considered in [5], where an external loop focuses on the reconfiguration of the system, while an inner loop handles the tensions in the cables.

A constrained model predictive controller, based on the linearization of the dynamic model, has been reported in [6]. Bounded torques of the actuators are guaranteed according to the controller constrains and through a tension distribution algorithm.

The computed-torque control (CTC) strategy together with proportional-derivative (PD) or proportional-integral-derivative (PID) controllers, have been reported by several authors [7]-[11] for a trajectory tracking task.

The CTC scheme, based on feedback linearization, allows a system to perform trajectory tracking with acceptable results. In [7], the correct selection of the controller parameters guarantees an asymptotically stable tracking error with an exact knowledge of the system parameters and in the absence of disturbances. When considering uncertainties in the system parameters and in the presence of disturbances, a bounded tracking error is obtained. These results are obtained from numerical simulations.

The work presented in [9], proposes a CTC scheme to generate a desired wrench based on a system dynamic model. The necessary forces to generate the desired wrench are chosen according to predefined stiffness values. The authors reported a non-desired behavior when performing trajectory tracking tasks due to negative stiffness values. This situation could imply the loss of tension in the tensegrity system.

The use of a static model to compute the set of possible forces applied for each equilibrium position is reported in [11]. A CTC with a PID correction is used to compute the two forces to generate the actuation wrench by neglecting Coriolis effects since the motion at low speeds is considered. In addition, friction effects are neglected too.

Unmodeled dynamics such as inertia effects due to neglected masses ([7] and [9]) or friction in joints or pulleys ([8], [9] and [11]) cause errors and unwanted behaviors.

The SMC approach is a robust technique to deal with external disturbances, unmodeled dynamics, and parametric uncertainties [12]. SMC strategies have been applied to different system types including nonlinear systems, multiple input/multiple output systems, discrete-time models, large-scale and infinite-dimensional systems, and stochastic systems [13]. Within SMC, the system states are forced to reach and move through a predefined sliding surface. Hence, the system dynamics is determined by this surface instead of being influenced by uncertainties or disturbances. This approach allows the dynamic performance of the system to be fixed [14].

To the best of the authors' knowledge, the control of tensegrity systems using the SMC approach has not yet been reported. Then, the main contribution of this paper concerns the implementation and experimental validation of the sliding mode strategy to control the position and the stiffness of this kind of systems. Simulation test followed by experimental validations of the control strategy with and without external disturbances are conducted on a planar one degree of freedom

(DOF) tensegrity system. Stability analysis of the control approach is performed.

This paper is organized as follows. Section II presents the dynamic modeling of the 1DOF rotational tensegrity system (RTS). Section III focuses on the sliding mode control design that is synthesized for the RTS. Section IV provides the stability analysis of the system under the proposed control strategy. Section V presents the tension distribution algorithm that allows the generation of two desired forces to apply a desired torque to the system. In Section VI, numerical simulations and experimental results are reported together with the validation of the effectiveness of the strategy under external disturbances. Conclusions of this work are finally presented in Section VII.

II. TENSEGRITY SYSTEM MODELING

An *n*-th order tensegrity system has a generalized coordinates vector $\mathbf{q} = [q_1 \ q_2 \ \cdots \ q_n]^T$ where q_i, i=1, 2, ⋯, n represents the i-th independent coordinate involved in the configuration definition of the system. The first- and second-time derivatives of this i-th coordinate are represented by $\dot{q}_i$ and $\ddot{q}_i$, respectively. When a Lagrange formulation is used to model the system of interest, the following energies need to be considered: the rotational kinetic energy $E_{KR}(\dot{q}_i)$, the translational kinetic energy $E_{KT}(\dot{q}_i)$, the gravitational potential energy $E_{GP}(q_i)$, and the elastic potential energy $E_{EP}(q_i)$. Then, the Lagrangian L of the tensegrity system takes the form:

$$L(q,\dot{q})=[E_{KR}(\dot{q}_i)+E_{KT}(\dot{q}_i)]-[E_{GP}(q_i)+E_{EP}(q_i)]$$

The Euler-Lagrange equations of motion of the n-th order tensegrity system, are obtained according to:

$$\frac{d}{dt}\frac{\partial L}{\partial \dot{q}_i}-\frac{\partial L}{\partial q_i}=Q_i \tag{1}$$

where Q_i represents the generalized force related with the i-th generalized coordinate. This set of differential equations can be represented in this compact form:

$$\mathbf{M(q)}\ddot{\mathbf{q}}+\mathbf{C}(\mathbf{q},\dot{\mathbf{q}})\dot{\mathbf{q}}+\mathbf{G}(\boldsymbol{q})=\mathbf{Q(u)} \tag{2}$$

where $\mathbf{M(q)}$ is the $n\times n$ positive definite symmetric inertia matrix, $\mathbf{C(q,\dot{q})\dot{q}} \in \mathrm{R}^n$ groups the Coriolis and centrifugal effects, $\mathbf{G(q)} \in \mathrm{R}^n$ is the vector of conservative forces and $\mathbf{Q(u)} \in \mathrm{R}^n$ is the vector of generalized forces that depends on the input $\mathbf{u} \in \mathrm{R}^p$. For the set of n state variables provided in (3), the dynamic of the n-th order tensegrity system can be defined by the set of 2n differential equations in (4), where j=0, 1, 2, ⋯, n-1.

$$\begin{cases} x_1=q_{j+1} \\ x_2=\dot{q}_1 \end{cases} \tag{3}$$

$$\begin{cases} \dot{x}_{2j+1}=x_{2j+2} \\ \dot{x}_{2j+1}=x_{2j+2} \end{cases} \tag{4}$$

The elements $\ddot{q}_{j+1}$ are the components of the vector $\ddot{\mathbf{q}}=[\ddot{q}_1 \ \ddot{q}_2 \ldots \ddot{q}_n]^T$.

The interest of this paper is in the design of a closed-loop super twisting control strategy that, for a tensegrity system, guarantees stability as well as small errors with respect to a reference signal. The design of a super twisting controller for this kind of systems is applied to a planar tensegrity device that is modeled using the Lagrangian approach.

The tensegrity system under study is a four-bar linkage. All bars have the same length l and mass m. Their joints are located at the points A, B, C and D (see Fig. 1a). This parallelogram is driven by two rotary actuators through two rigid cables attached to the points B and C at one end and to the springs 1 and 2, on the other end. It is assumed that both springs are homogeneous and have the same stiffness constant k. The system angular position is defined by θ. Since the system is under a prestressed condition, θ=θ(F_1,F_2) where F_1 and F_2 are the tension in the cables BD and CA, respectively.

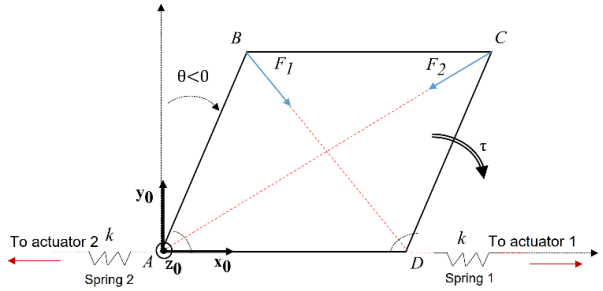

a) Rotational tensegrity system representation.

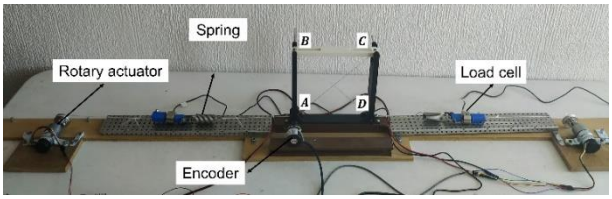

b) Rotational tensegrity system experimental platform.

Fig. 1. *One DOF rotational tensegrity mechanism.*

Fig. 1b illustrates the RTS experimental platform. Two rotary actuators generate the displacements of cables BD and CA and, consequently, the angular motion of the system. A rotary encoder, placed at the joint in A, provides information on the parallelogram angular position. Two load cells are integrated to the cable transmission to measure the tensions in the cables.

In order to reduce friction, bearings are mounted in each bar joint. Pulleys with bearings are also used. The main differences between the mechanism under study in this paper and the mechanism reported in [15] are presented in Table I.

TABLE I. *MECHANISM DIFFERENCES.*

Characteristic	**New design**	**[15] system**
Bars length	21 cm	7 cm
Bar mass	80 g	10 g
Number of cables	3	4
Joints	Bearings	Polymer
Bars material	Polylactic acid	Polymer

A dynamic model developed using a Lagrangian approach of the RTS, is provided in (5) where C_1, C_2 and C_3 are physical parameters, $\dot{\theta}$ and $\ddot{\theta}$ are, respectively, the first and the second time derivatives of θ.

$$C_1\ddot{\theta}+C_2\dot{\theta}+C_3\sin\theta=F_2 l\sin\left(\frac{90+\theta}{2}\right)-F_1 l\cos\left(\frac{90+\theta}{2}\right) \quad (5)$$

The right side of (5) represents the extern generalized torques generated by the forces F_1 and F_2. This model includes the viscous friction in each flexible joint as an external torque to the system, represented by the term $C_2\dot{\theta}$. It is highlighted that $\theta<0$ implies a clockwise angular motion (see Fig. 1a) and that the applied total torque vector is parallel to the respective $\mathbf{z_0}$ axis.

III. Sliding Mode Control Strategy

The mechanism presented in Fig. 1 is an overactuated system since two forces F_1 and F_2 generate a single torque τ providing an angular motion. The super twisting SMC strategy is depicted in Fig. 2. It allows to control the output of the system θ_m with respect to the reference θ_{ref}. The controller generates a signal τ_d that represents the desired virtual torque. This signal is used as input to a tension distribution algorithm, developed by [16], that generates the reference forces $\mathbf{F}^*=\begin{bmatrix}F_1^* & F_2^*\end{bmatrix}^T$.

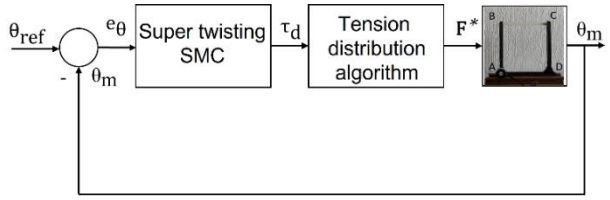

Fig. 2. *SMC control strategy.*

In order to synthesize a SMC strategy for the reported RTS, a state space representation of the model in (5) is provided in (6). First time derivative of $\mathbf{x}$ is represented by $\dot{\mathbf{x}}$.

$$\dot{\mathbf{x}}=\mathbf{A}\mathbf{x}+\bar{\mathbf{f}}(\mathbf{x})+\bar{\mathbf{g}}(\mathbf{x})\tau_d \quad (6)$$

where:

$$\mathbf{x}=\begin{bmatrix}x_1\\x_2\end{bmatrix}=\begin{bmatrix}\theta\\\dot{\theta}\end{bmatrix} \qquad \mathbf{A}=\begin{bmatrix}0 & 1\\0 & -\frac{C_2}{C_1}\end{bmatrix}$$

$$\bar{\mathbf{f}}(\mathbf{x})=\begin{bmatrix}0\\f(\mathbf{x})\end{bmatrix} \qquad \bar{\mathbf{g}}(\mathbf{x})=\begin{bmatrix}0\\1/C_1\end{bmatrix}$$

The control signal τ_d corresponds to the torque required to reach a desired position and is associated to the springs' forces F_1 and F_2. The vector $\bar{\mathbf{f}}(\mathbf{x})$ contains the scalar nonlinear function:

$$f(\boldsymbol{x})=2mgl\sin(\theta) \quad (7)$$

where g represents the gravitational acceleration. The proposed control strategy consists of two phases. The first one, is the reaching phase (u_{st}) that attracts the state variables of the system to a desired sliding surface. The second phase is an equivalent control (u_{eq}) that maintains the system on the sliding surface.

The super-twisting algorithm acts directly on the second-time derivative of the sliding variable $\mathbf{x_s}$, defined in (10), and has been reported as simple to implement [17].

The reaching super-twisting control law (u_{st}) is provided by (8), were α_1 and α_2 are the control gains and S is the sliding surface defined in (9).

$$u_{st}=\alpha_1|S|^{\frac{1}{2}}\text{sign}(S)+Z \quad (8)$$

with $\dot{Z}=\alpha_2\text{sign}(S)$.

$$S=\boldsymbol{K}\boldsymbol{x_s} \quad (9)$$

$\mathbf{K}=[K_1 \;\; 1]$ is a row vector with a constant $K_1\in\mathrm{R}$, and $\mathbf{x_s}$ represents the sliding variable. Its expression is given by:

$$\mathbf{x_s}=\begin{bmatrix}x_1-x_{1ref}\\x_2\end{bmatrix}=\begin{bmatrix}\theta-\theta_{ref}\\\dot{\theta}\end{bmatrix} \quad (10)$$

where $x_{1ref}=\theta_{ref}$ is the desired angular position. Once the control u_{st} is obtained, an equivalent control u_{eq} is derived. The system states remain in the sliding surface if condition (11) is satisfied [13]:

$$\mathbf{K}\frac{d}{dt}S=0 \quad \text{when} \quad S=0 \quad (11)$$

Considering the equivalent control in (12), (11) is satisfied.

$$u_{eq}=\begin{cases}-\dfrac{\mathbf{K}[\mathbf{A}\mathbf{x}+\bar{\mathbf{f}}(\mathbf{x})]}{\mathbf{K}\bar{\mathbf{g}}(\mathbf{x})} & \text{if } \bar{\mathbf{g}}(\mathbf{x})\neq 0\\ 0 & \text{else}\end{cases} \quad (12)$$

The regulation task for the system provided in (6) is achieved by using the SMC defined in (13), where u_{st} and u_{eq} are defined respectively by (8) and (12):

$$\tau_d=u_{st}+u_{eq} \quad (13)$$

IV. Stability Analysis

The control law in (13) constrains the system states to reach and stay on the sliding surface. Then, the stability analysis of the controlled nonlinear system focuses on both the reaching and the sliding phases.

During the reaching phase, condition $S\neq 0$ is fulfilled. Consider the positive definite Lyapunov function:

$$V=\frac{1}{2}S^2 \quad \text{for} \quad S\neq 0 \quad (14)$$

and its time derivative:

$$\dot{V}=S\dot{S}=\mathbf{K}\mathbf{x_s}\mathbf{K}\dot{\mathbf{x}} \quad (15)$$

Considering (6), and (13), $\dot{V}$ in (15) takes the form:

$$\dot{V}=\mathbf{K}\mathbf{x_s}\mathbf{K}[\mathbf{A}\mathbf{x}+\bar{\mathbf{f}}(\mathbf{x})]+\mathbf{K}\mathbf{x_s}\mathbf{K}\bar{\mathbf{g}}\left[u_{st}+u_{eq}\right] \quad (16)$$

Substituting (8) and (12) into (16) and by simplifying terms, (17) is obtained as:

$$\dot{V}=S\mathbf{K}\bar{\mathbf{g}}\left[\alpha_1|S|^{\frac{1}{2}}\,\mathrm{sign}(S)+Z\right] \quad (17)$$

where $Z=\int_0^h \alpha_2 \mathrm{sign}(S)\,dt$, with h a finite time. Solving the integral $Z=\alpha_2 \mathrm{sign}(S)h$.

Substituting Z into (17), the time derivative of the Lyapunov function can be re-written as:

$$\dot{V}=\alpha_1|S|^{\frac{1}{2}}|S|\mathbf{K}\bar{\mathbf{g}}+\alpha_2|S|\mathbf{K}\bar{\mathbf{g}}h \quad (18)$$

where $h>0$ and $\mathbf{K}\bar{\mathbf{g}}>0$. When the control gains $\alpha_1<0$ and $\alpha_2<0$, $\dot{V}$ is negative definite and the closed-loop system, during the reaching phase of the control strategy, is asymptotically stable.

During the sliding phase, the system states remain in the sliding surface and condition (19) is satisfied:

$$S=\mathbf{K}\mathbf{x_s}=0 \quad (19)$$

Substituting (10) into (19), the differential equation (20) is obtained:

$$K_1 x_{ref} - K_1 x_1 = \dot{x}_1 \quad (20)$$

This equation describes the system behavior during the sliding phase. The solution of (20) and its derivative are given by:

$$\begin{cases} x_1=x_{ref}-C_0 e^{-K_1 t} \\ \dot{x}_1=x_2=-K_1 C_0 e^{-K_1 t} \end{cases} \quad (21)$$

where $K_1>0$ and C_0 is a constant associated with the initial configuration of the system. The state x_1 converges exponentially to the reference state and the state x_2 converges exponentially to zero. The system is therefore exponentially stable during the sliding phase.

Since exponential stability implies asymptotic stability [18], one can conclude that the system in closed-loop configuration is asymptotically stable.

V. Tension Distribution Algorithm

The desired virtual torque τ_d, generated by the SMC strategy, is transformed into a pair of desired tensions F_i^* in the cables. In order to guarantee that these desired tensions evolve in accordance with the real tensions $\mathbf{F^m}=[F_1 \;\; F_2]^T$, a PID controller is implemented, as illustrated in Fig. 5.

The tension distribution algorithm uses the desired torque generated by the SMC strategy to obtain the reference tensions in the springs $\mathbf{F}^*=\left[F_1^* \;\; F_2^*\right]^T$ to be applied. These tensions are obtained by solving the constrained linear system in (22):

$$\begin{cases} \mathbf{W}\mathbf{F}^*=\tau_d \\ \text{such that: } \mathbf{F_{min}}<\mathbf{F}^*<\mathbf{F_{max}} \end{cases} \quad (22)$$

where $\mathbf{W}=[-l\cos(\frac{90+\theta}{2}) \;\; l\sin(\frac{90+\theta}{2})]$. This algorithm must ensure a positive bounded force in each spring to maintain a positive stiffness in the tensegrity mechanism. To do so, a positive bounded interval $[\mathbf{F_{min}};\mathbf{F_{max}}]$ is defined where $\mathbf{F_{min}}=[F_{1min} \;\; F_{2min}]^T$ and $\mathbf{F_{max}}=[F_{1max} \;\; F_{2max}]^T$ are the admissible minimal and maximum forces in each spring. The solution of (22) takes the form [16]:

$$\mathbf{F}^*=\mathbf{W}^+\tau_d+\mathbf{N}_w\lambda \quad (23)$$

where $\mathbf{N_w}=\left[-l\sin(\frac{90+\theta}{2}) \; -l\cos(\frac{90+\theta}{2})\right]^T$ is the basis of $\mathbf{W}$ null space. $\mathbf{W}^+$ is the Moore–Penrose pseudoinverse of $\mathbf{W}$ and $\lambda \in R$ satisfies:

$$\mathbf{F_{min}}-\mathbf{W}^+\tau_d \le \mathbf{N}_w\lambda \le \mathbf{F_{max}}-\mathbf{W}^+\tau_d \quad (24)$$

The set $B=\{\lambda|\lambda_{min}\le\lambda\le\lambda_{max}\}$ is computed using the inequality in (24). The value of λ can be chosen as $\lambda=(\frac{\lambda_{min}+\lambda_{max}}{2})$.

This approach allows to maintain the forces in the springs as far as possible from the maximum and the minimum values according to the mechanism orientation. These forces reproduce the desired torque generated by the SMC to be applied to the system in order to reach the reference orientation.

VI. Numerical Simulations and Experimental Tests

A. Numerical simulations

Closed-loop numerical simulations are carried out to evaluate the control strategy depicted in Fig. 2. The simulation parameters of the RTS are reported in Table II.

TABLE II. *Parameters.*

Parameter	Value	Units
Bars length	0.21	m
Bars mass	0.015	kg
Springs constant	219	N/m
Constant C_1	7.4×10^{-4}	kg m^2
Constant C_2	-0.04	kg m^2/s
Constant C_3	0.6174	Nm
$\mathbf{F_{min}}$	[2 2]	N
$\mathbf{F_{max}}$	[20 20]	N

The minimum admissible force in each spring was selected to always guarantee a positive tension in the cables. The maximum admissible force was selected to avoid oversizing the actuators.

The control strategy performance depends on the values of the gains K_1, α_1 and α_2. For simulations and experimental tests, the system initial position is $\theta_0=0°$. This condition guarantees a stable position of the mechanism in absence of external disturbances.

A trajectory that reaches θ_{ref}=-45° in 1 second using a sigmoid function is considering to analyze the performance of the control strategy. The controller gains are selected heuristically depending on the stability analysis reported in Section IV. The behavior of the output signal is observed in Fig. 3 (red line) together with the reference trajectory (black line).

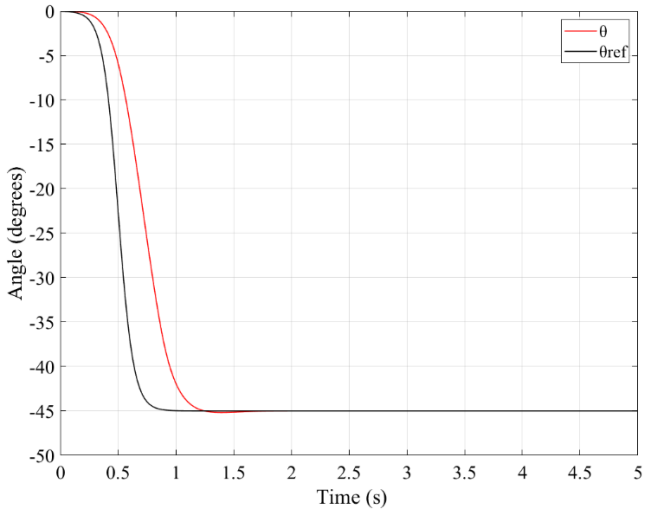

Fig. 3. Behavior of θ ($K_1 = 12$, $\alpha_1 = -0.0045$, $\alpha_2 = -0.01$).

In Fig. 3, a tracking error is observed during the transient response. Nevertheless, the steady state error e_{ss}=0°. The gain values of the super twisting SMC are K_1=12, α_1=-0.0045 and α_2=-0.01. The springs forces behaviors are shown in Fig. 4. Forces on both springs remain positive and between the admissible minimal (2 N) and maximum (20 N) tensions.

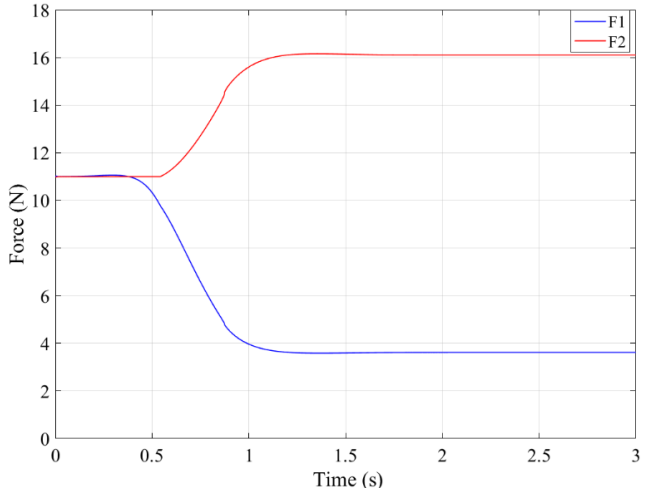

Fig. 4. Forces behavior ($K_1 = 12$, $\alpha_1 = -0.0045$, $\alpha_2 = -0.01$).

B. *Experimental tests*

To validate the proposed control approach, experimental tests were carried out using a STM32-NUCLEO board with a STM32F746ZGT6 ARM Cortex M7 microcontroller. An incremental encoder (LPD3806-400BM-G5-24C) with a resolution of 0.22°, coupled with the experimental platform, is considered to measure the angular position of the RTS. Two DC motors (GB37Y3530-12V-251R) are used to generate the desired forces in each spring (see Fig. 1b).

The implementation of the control strategy was performed using the Rapid Control Prototyping methodology described in [19]. This methodology facilitates the programming of complex control systems in microcontrollers.

As it has been mentioned previously, an inner control loop with a PID controller in considered to control the desired forces (see Fig. 5).

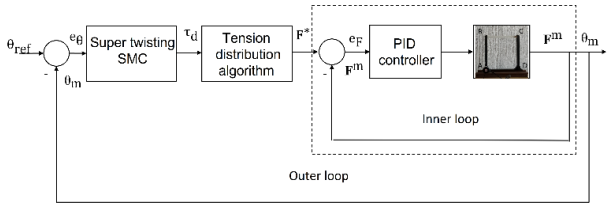

Fig. 5. Experimental test control strategy.

The gains of the PID controller, used to control the springs' forces, have been tuned experimentally and chosen equal to K_p=710, K_i=0.001, and K_d=600. Initial forces in the springs equal 11 N, that is the mean value between the selected $\mathbf{F_{min}}$ and $\mathbf{F_{max}}$,have been applied. Initial conditions for these experimental tests are θ_0=0° and $\dot{\theta}_0$=0°.

The parameters of the experimental platform have the same values used for the numerical simulations (see Table II). The system behavior (red line) is observed in Fig. 6 when performing experimental tests with controller gains K_1=12.8, α_1=-0.3, and α_2=-0.06. The reference trajectory is the same as the one used in numerical simulations.

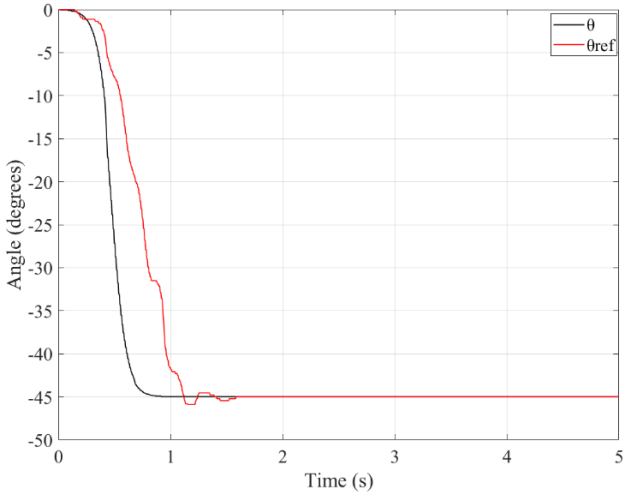

Fig. 6. Experimental response of θ ($K_1 = 12.8$, $\alpha_1 = -0.3$, $\alpha_2 = -0.06$).

The mechanism reaches the final stable position with 0°<e_{ss}<0.22°. The forces in the cables are illustrated in Fig. 7. As it can be observed, the tensions in the cables remain positive and within the admissible range.

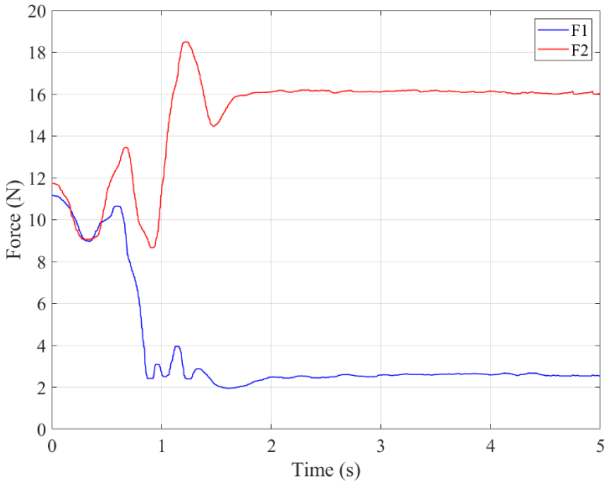

Fig. 7. Springs forces behavior ($K_1 = 12.8$, $\alpha_1 = -0.3$, $\alpha_2 = -0.06$).

As it can be observed, the experimental results related to trajectory tracking follow the tendency shown in the numerical simulations.

C. *Stiffness modulation*

The capacity of the system to counteract the effect of external forces is directly related to its stiffness [20]. The stiffness of the system in a stable configuration is defined [6] as:

$$K_\theta = -\frac{\partial \tau_d}{\partial \theta} \tag{25}$$

Including (22) and considering the effect associated to the potential energy of the bars, the system stiffness can be calculated as:

$$K_\theta = -2mgl\cos(\theta) - \frac{l}{2}\left[F_2\cos\left(\frac{90+\theta}{2}\right) + F_1\sin\left(\frac{90+\theta}{2}\right)\right] + kl^2 \tag{26}$$

By modifying the value of λ in the tension distribution algorithm between $\lambda_{min} \leq \lambda \leq \lambda_{max}$, one can change the forces in the springs (23) without affecting the orientation of the RTS. Indeed, the variation of λ allows the variation of the internal forces in the system, which will directly affect the system stiffness.

A desired position θ_{ref}=-30° is established to perform a stiffness variation experiment by generating abrupt changes in the value of λ to modify the stiffness of the tensegrity system. The value of λ during the interval $0 \leq t < 4$ s is calculated by $\lambda = \left(\frac{\lambda_{min}+\lambda_{max}}{2}\right)$. At t=4 s, the value of λ decreases to its minimum admissible value λ_{min}, in consequence the forces F_1 and F_2 present an increment (see Fig. 8). At t=9 s, the value of λ returned to its mean value. At t=14 s, the value of λ increase to its maximum admissible value λ_{max} causing a decrement in forces F_1 and F_2 as it can be observed in Fig. 8.

These variations are highlighted with vertical dotted lines 1, 2, and 3. These changes in the values of λ modify the solution of (23) and consequently the forces F_1 and F_2 to apply the desired torque τ_d.

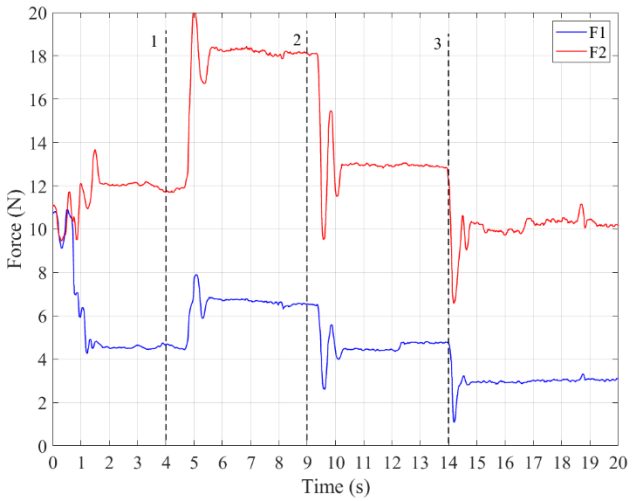

Fig. 8. Springs forces behaviors when changing the stiffness.

The variations in the forces F_1 and F_2 are associated with the actions of the control signals to maintain the desired angular position (see Fig. 8 and Fig. 9). The changes in the forces F_1 and F_2 observed in Fig. 8, modify the level of stress in the cables of the system and, consequently, the stiffness of the RTS.

As it can be observed in Fig. 9, the controller reacts to the variations of λ at times t=4 s, t=9 s, and t=14 s with the objective of conserving the system at the desired position (θ_{ref}=-30°) even when the forces in the springs are changing. This is mainly due to the fact that the changes in the internal forces $\mathbf{F}^*$ is performed in the null space of $\mathbf{W}$ by changing the value of λ (23).

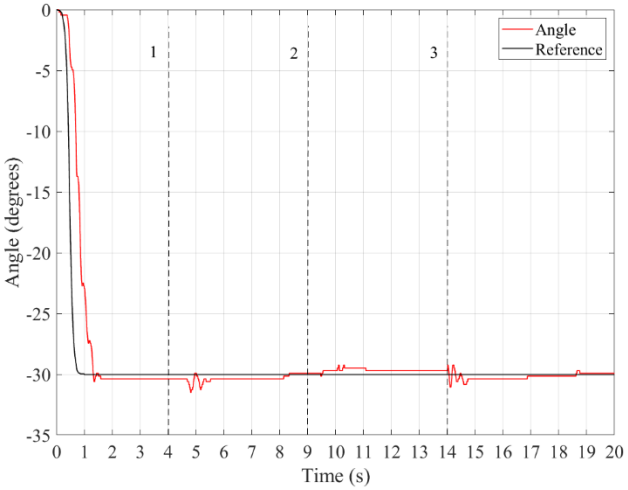

Fig. 9. System behavior during stiffness modulation.

The stiffness behavior is shown in Fig. 10. It is computed using (26) and considering experimental data. The changes on the forces observed in Fig. 8 are directly associated with the stiffness modulation represented in Fig. 10 (see dotted lines 1, 2, and 3). As it can be seen in Fig. 8 and Fig. 10, the force in each spring and, in consequence, the system stiffness values remain almost constant, when the value of λ is not modified.

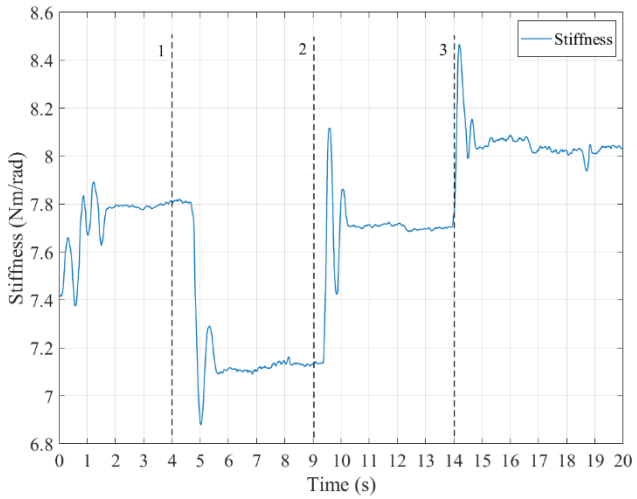

Fig. 10. Stiffness variation during experiments.

One of the advantages of tensegrity systems is the property they have to modulate their stiffness as it is shown in Fig. 10, where this modulation was performed in a closed-loop configuration using a super twisting controller.

D. Robustness against external disturbances.

The robustness of the control strategy with respect to external perturbations is experimentally evaluated. Once the mechanism reaches its stable position, a series of six external disturbances is applied to the system.

The amplitudes of these disturbances vary from 15° to 20° and are applied at 6 s, 10.1 s, 16 s, 19.9 s, and 23.8 s. The response of the closed-loop system under the effect of these disturbances is shown in Fig. 11.

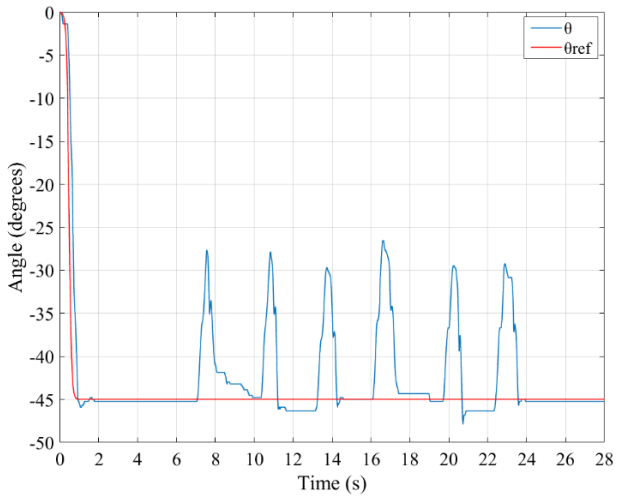

Fig. 11. System behavior in presence of external disturbances.

As it can be observed in Fig. 11, the action of the super-twisting control strategy returns the mechanism to its stable position once the disturbance disappears, thus validating the robustness of the proposed control strategy.

The forces behavior, when external disturbances are applied to the system, are shown in Fig. 12. Again, as it can be observed the system maintains a positive force in each spring in the presence of external disturbances. The variations of the spring's forces highlight the antagonistic configuration of the tensegrity system (the force F_1 increases when the force F_2 decreases and vice versa).

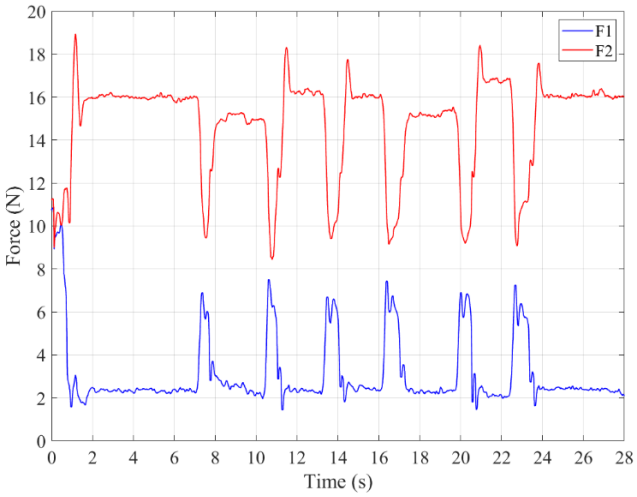

Fig. 12. Force behavior in the presence of external disturbances.

Fig. 13 shows the behaviors of the actuators when the external disturbances are applied to the system. The control strategy reacts to the non-measured disturbances by moving the actuators and, in consequence, changing the springs' forces that generate the required torque to relocate the system in the desired position. The displacements in the rotary actuators 1 and 2 are directly related, respectively, to the changes in the forces in springs 1 and 2 (see Fig. 1b).

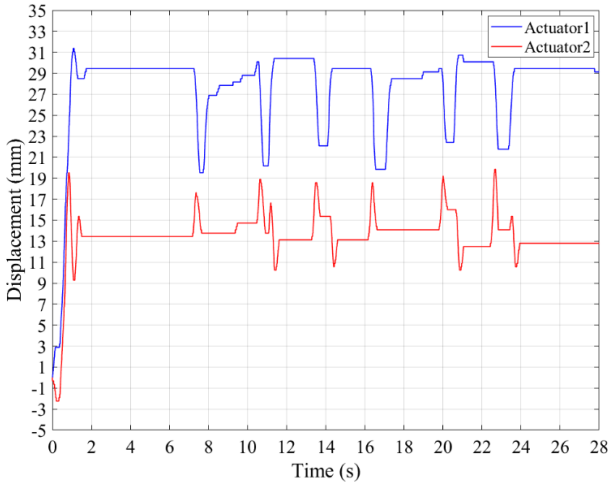

Fig. 13. Actuarors' displacements under external disturbances.

VII. Conclusions

A super-twisting sliding mode control strategy for a planar tensegrity mechanism has been reported in this paper. This control strategy is applied to a nonlinear dynamic model of the tensegrity mechanism of interest with the objective to drive the system to a desired angular position.

A tension distribution algorithm ensures a positive bounded force in each spring, guaranteeing the prestressed

condition of the tensegrity system. The effectiveness of this control strategy has been verified with numerical simulations and validated through experimental tests. Experiments in a physical platform show an acceptable steady state error less or equal to the encoder resolution. Moreover, experimental validation of the capacity of the control strategy to modify the stiffness of the system has been demonstrated.

Besides, closed-loop stability has been proved for both the reaching and the sliding phases of the proposed SMC strategy.

The robustness of the control strategy against external disturbances was, experimentally, validated with satisfactory results. Once the external disturbances disappear, the controller is capable to return the system to the reference position without losing the tension in the springs and then, preserving the prestress condition that characterizes tensegrity systems.

REFERENCES

[1] A. S. Wroldsen, "Modelling and Control of Tensegrity Structures", Diss. Department of Marine Technology, Norwegian University of Science and Technology, 2007.

[2] R. Motro, "*Tensegrity: Structural Systems for the Future",* Sterling VA: Kogan Page Science, London, 2003.

[3] Q. Boehler, A. Zompas, S. Abdelaziz, M. Vedrines, P. Poignet, P. Renaud, "Experiments on a variable stiffness tensegrity mechanism for an MR-compatible needle holder", CRAS: Computer/Robot Assisted Surgery, , Bruxelles, Belgium, Sep 2015.

[4] A. González, A. Luo, "Design and Control of a Tensegrity-Based Robotic Joint", in: Advances in Mechanism and Machine Science. IFToMM WC Mechanisms and Machine Science, vol 73, T. Uhl, Eds, Springer, 2019.

[5] Q. Boehler, S. Abdelaziz, M. Vedrines, P. Poignet, P. Renaud, "From modeling to control of a variable stiffness device based on a cable-driven tensegrity mechanism", Mechanism and Machine Theory, Volume 107, 2017, pp 1-12.

[6] JR. J. Realpe, S. Abdelaziz and P. Poignet. "Model Predictive Controller for a Planar Tensegrity Mechanism with decoupled position and stiffness control", in: Advances in Robot Kinematics 2020, Springer Proceedings in Advanced Robotics, vol 15, Lenarčič J., Siciliano, Eds. Springer, 2020.

[7] R. E. Vasquez, J. C. Correa, "Kinematics, dynamics and control of a planar 3-dof tensegrity robot manipulator", International Design Engineering Technical Conferences & Computers and Information in Engineering Conference, USA, 2007.

[8] B. Fasquelle, M. Furet, C. Chevallereau, and P. Wenger, "Dynamic modeling and control of a tensegrity manipulator mimicking a bird neck", Advances in Mechanism and Machine Science, Mechanisms and Machine Science 73, Springer Nature Switzerland AG 2019.

[9] A. van Riesen, M. Furet, C. Chevallereau, and P. Wenger "Dynamic Analysis and Control of an Antagonistically Actuated Tensegrity Mechanism", Robot Design, Dynamics and Control, pp. 481–490, 2019.

[10] A. Balon, Z. Šika, "Optimization and control of mechatronic tensegrity for robotics", Computational Mechanics 35th conference with international participation, November 2019.

[11] B. Fasquelle, M. Furet, P. Khanna, D. Chablat, Ch. Chevallereau, P. Wenger, "A bio-inspired 3-DOF light-weight manipulator with tensegrity X-joints", ICRA'2020, Paris, France, May 2020.

[12] H. Sira-Ramírez, "Sliding mode control: the delta-sigma modulation approach", Control Engineering, Birkhüauser Basel. 2015.

[13] J. Y. Hung, W. Gao and J. C. Hung, "Variable structure control: a survey," in *IEEE Transactions on Industrial Electronics*, vol. 40, no. 1, pp. 2-22, Feb. 1993.

[14] B. Saldivar, J. C. Avila Vilchis, A. H. Vilchis González, Edgar Martínez Marbán, "Sliding Mode Control for a Class of Control-Afine Nonlinear Systems", Control Engineering and Applied Informatics, Vol.20, No. 3, pp. 3-11, 2018.

[15] Q. Boehler ,S. Abdelaziz,M. Vedrines, P. Poignet,P. Renaud, "Towards the Control of Tensegrity Mechanisms for Variable Stiffness Applications: A Case Study" in: New Trends in Mechanism and Machine Science. Mechanisms and Machine Science, vol 43, P. Wenger, P. Flores, Eds. Springer, 2017.

[16] M. Gouttefarde, J. Lamaury, C. Reichert and T. Bruckmann, "A Versatile Tension Distribution Algorithm for n-DOF Parallel Robots Driven by n+2 Cables," in *IEEE Transactions on Robotics*, vol. 31, no. 6, pp. 1444-1457, Dec. 2015.

[17] D. Matouk, F. Abdessemed, O. Gherouat and Y. Terchi, "Second-order sliding mode for position and attitude tracking control of quadcopter uav: super-twisting algorithm", International Journal of Innovative Computing, Information and Control, Vol. 16, No. 1, pp. 29-33, 2020.

[18] J.-J. Slotine and L. Weiping, "Applied Nonlinear Control", Englewood Cliffs, N.J.: Prentice Hall, 1991.

[19] J. M. Jacinto-Villegas, O. Portillo-Rodríguez, R. Martínez-Méndez, A. H Vilchis-González, C. A. Daza-Merino, J. C. Avila Vilchis, "Sistema para control de posición basado en Rapid Control Prototyping (RCP) usando Simulink y SWB32", Sociedad Mexicana de Inteligencia Artificial, Komputer Sapiens, ISSN 2007-0691, Año XI, Vol. III, pp. 11-15, diciembre 2019.

[20] M. Arsenault, C. M. Gosselin, "Kinematic, static and dynamic analysis of a planar 2-DOF tensegrity mechanism" Mechanism and Machine Theory, vol. 41, Issue 9, pp. 1072-1089, 2006.